

# Black hole image encoding quantum gravity information

Cong Zhang<sup>1,\*</sup> Yongge Ma,<sup>2,†</sup> and Jinsong Yang<sup>3,‡</sup>

<sup>1</sup>*Department Physik, Institut für Quantengravitation, Theoretische Physik III,  
Friedrich-Alexander-Universität Erlangen-Nürnberg, Staudtstraße 7/B2, 91058 Erlangen, Germany*

<sup>2</sup>*Department of Physics, Beijing Normal University, Beijing 100875, China*

<sup>3</sup>*School of Physics, Guizhou University, Guiyang 550025, China*

The quantum extension of the Kruskal spacetime indicates the existence of a companion black hole in the universe earlier than ours. It is shown that the radiations from the companion black hole can enter its horizon, pass through the deep Planck region, and show up from the white hole in our universe. These radiations inlay extra bright rings in the image of the black hole in our universe, and some of these rings appear distinctly in the shadow region. Therefore, the image of the black hole observed by us encodes the information of quantum gravity. The positions and widths of the bright rings are predicted precisely. The predictive values for supermassive black holes are universal for a quite general class of quantum modified spacetime with the scenario of black hole to white hole transition. Thus, our result opens a new experimental window to test this prediction of quantum gravity.

One of the most challenging topics in modern physics is how to unify quantum mechanics and general relativity. While there are many efforts to this end through theoretical considerations (see, e.g., [1–3]), a severe obstacle blocking the construction of a viable theory of quantum gravity (QG) is the lack of experimental data. On one hand, it is argued that the detection of a graviton could be unrealistic [4, 5]. On the other hand, it is proposed to detect the QG effects by the entanglement between massive particles [6], Lorentzian invariance violation [7], and other QG phenomenology [8].

Since the gravitational waves were detected by the LIGO/Virgo [9] and the BH images were photographed by the Event Horizon Telescope [10, 11], it has attracted extensive attention to probe the effects of QG by the observation on BHs [12–16]. However, the QG effects studied so far are tiny since they usually concern the physical processes in the classical region outside the BH horizon. Actually, the signals from a BH could bring on the information of QG only if they came from some highly quantum region inside the horizon. Classically, this can not happen since those signals inside the horizon will inevitably get to the singularity. However, the quantum extension of a BH spacetime indicates that the classical singularity can be resolved and there are a series of universes other than ours where companion BHs exist [17–19]. On this ground, as we will show in this letter, light signals can enter the horizon of the companion BH in the universe earlier than ours, travel through the highly quantum region, and occur in the image of the BH in our universe. More precisely, these lights inlay extra bright rings in the image of the BH, and some of them appear distinctly in the classical shadow region. The positions and widths of the bright rings can be predicted precisely. Remarkably, these predictive values for supermassive BHs are universal for a quite general class of quantum modified spacetime with the scenario of BH to white hole (WH) transition. Thus, our result opens a new experimental window to test this fantastic prediction of QG. Moreover, the next-to-leading order of the predictive values is model-dependent and thus encodes the information to distinguish different candidate theories.

A few quantum extensions of the Kruskal spacetime have been proposed in the study of loop quantum gravity (LQG)[17–30]. While the model in [19] will be employed in the following calculation, our analysis is valid for all these quantum spacetimes where a BH to WH transition occurs. The metric of the LQG modified spherically symmetric spacetime reads

$$ds^2 = -f(r)dt^2 + f(r)^{-1}dr^2 + r^2(d\theta^2 + \sin^2\theta d\varphi^2), \quad (1)$$

with

$$f(r) = 1 - \frac{2M}{r} + \frac{\alpha M^2}{r^4}, \quad \alpha = 16\sqrt{3}\pi\gamma^3\ell_p^2 \quad (2)$$

where the geometric unit with  $G = 1 = c$  is chosen such that  $\ell_p = \sqrt{\hbar}$  is the Planck length and  $\gamma$  denotes the Barbero-Immirzi parameter [31]. This modified spacetime was derived from two independent approaches in LQG [19, 32]. For realistic consideration, we assume that the BH is massive, i.e.,  $M \gg 4\sqrt{\alpha}/(3\sqrt{3})$ . In this case,  $f(r)$  has two real roots

\* czzhang(AT)fuw.edu.pl

† mayg(AT)bnu.edu.cn

‡ jsyang(AT)gzu.edu.cn

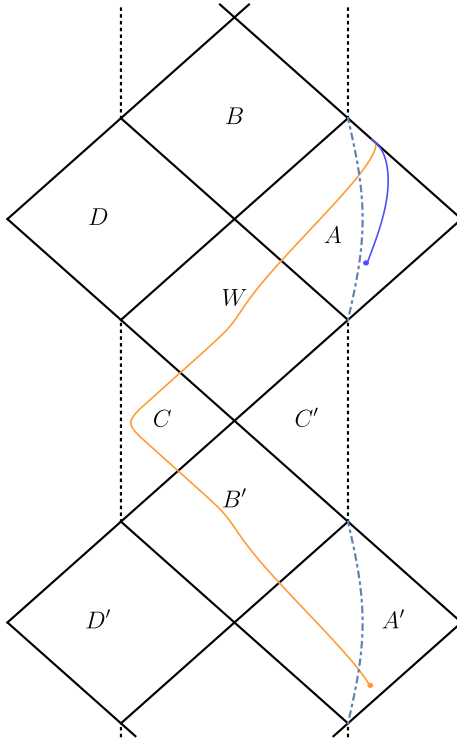


FIG. 1. The Penrose diagram of the quantum extended BH spacetime: The golden and blue lines are two null geodesics emitted from the thin disks in  $A'$  and  $A$  respectively and observed by the observer in Region  $A$  simultaneously. The dash-dotted blue line illustrates the location of the photon sphere.

$r_{\pm} > 0$ , corresponding to the two horizons in the maximally extended spacetime [19, 33], whose Penrose diagram is shown in Fig. 1.

Consider a static observer in the asymptotically flat region  $A$  near the future null infinity to detect the image of the companion BH  $B'$  and the BH  $B$  illuminated by distant, uniform, isotropically emitting screens surrounding them. Two null geodesics emitted by the screens surrounding  $B$  and  $B'$  are plotted by blue and golden lines respectively in Fig. 1. The image photographed by the observer should be the overlay of the images resulting from the “blue” and “golden” null geodesics. As the image produced by the geodesics of the blue lines has been given in [16], in the current work, we focus on the image from the golden geodesics and study their overlay.

With the Eddington–Finkelstein advanced coordinate  $(v_+, r, \theta, \varphi)$  in  $A' \cup B' \cup C$  and the retarded coordinate  $(v_-, r, \theta, \varphi)$  in  $C \cup W \cup A$ , the conservation equations of energy and angular momentum together with the vanishing norm of the null geodesics imply

$$\left( \frac{du}{d\phi} \right)^2 = -\alpha M^2 u^6 + 2Mu^3 - u^2 + \frac{1}{b^2} \equiv G(u, b), \quad (3)$$

where  $u \equiv 1/r$ ,  $\phi \in (0, \infty)$  is the azimuthal angle in the orbit plane, and  $b$ , the impact factor given by the ratio of the angular momentum and energy, is a constant of motion and chosen to be positive.

Equation (3) ensures  $G(u, b) \geq 0$  along the geodesics and implies that the turning points occur at the roots  $u$  of  $G(u, b)$ . It is easy to check that  $G(u, b) = 0$  allows at most four real roots and two of them always exist. One is negative and thus unphysically, while the other, denoted by  $u_0$ , is positive and satisfies  $u_0 > 1/r_-$ . Let  $b_c$  denote the value of the impact factor for which the remaining two roots are a double root  $u_{\text{ph}}$ . It turns out that  $r_{\text{ph}} = 1/u_{\text{ph}} > r_+$  characterizes the photon sphere and  $r(\phi) = r_{\text{ph}}$  represents unstable null geodesics. They are plotted as the dash-dotted blue lines in Fig. 1. The cases with  $b > b_c$  are not considered in the current work since these null geodesics either lie entirely outside the horizon  $r_+$  or are confined in some finite radius. For the case of  $b < b_c$  where the remaining two roots are both complex, the null geodesics start from  $r = \infty$ , cross the two horizons and turn back at  $1/u_0$ , as the golden line in Fig. 1.

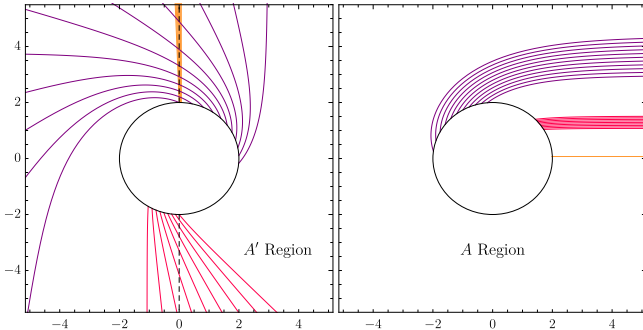


FIG. 2. The null geodesics for various impact factors:  $M$  is taken as the unit of radius. The circles plot the horizons  $r = r_+$ . The lines of same color represent the same geodesic congruence in the two regions respectively. The parameters are chosen as  $M = 243.75\sqrt{\alpha}$ ,  $\hbar = 1$  and  $\gamma = 0.2375$ . The values of  $b$  for the golden, red and purple geodesics lie in the intervals  $(b_1, b'_1) = (0.072M, 0.076M)$ ,  $(b_2, b'_2) = (1.077M, 1.512M)$  and  $(b_3, b'_3) = (2.974M, 4.373M)$  respectively.

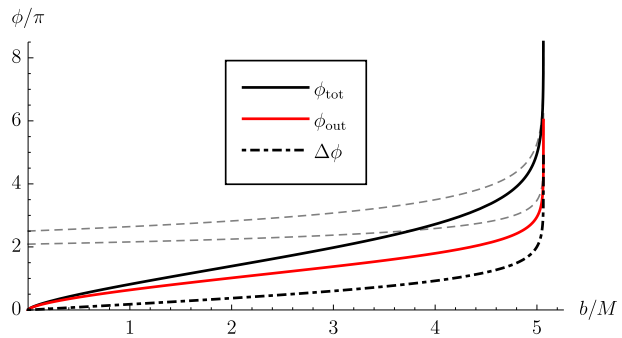


FIG. 3. The dependence of  $\phi_{\text{out}}$ ,  $\phi_{\text{tot}}$  and  $\Delta\phi = \phi_{\text{tot}} - \phi_{\text{out}}$  on  $b/M$ . The dashed gray line obtained by the analytical approximation (see Appendix B). The parameters are chosen as  $M = 243.75\sqrt{\alpha}$ ,  $\hbar = 1$  and  $\gamma = 0.2375$ .

To investigate the contribution of the geodesics with  $b < b_c$  to the BH image, we consider a model where the emissions originate from an optically and geometrically thin disk which stays at rest outside the BH  $B'$  and emits isotropically in the rest frame of the static observers [34, 35]. The disk is located in the equatorial plane as illustrated by a vertical black dashed line in the left panel of Fig. 2, and the observer in region  $A$  faces the north pole of the BH  $B$  in the right panel of Fig. 2. In this model, the relevant parts of each geodesic are those in Regions  $A$  and  $A'$ . The trajectories  $u(\phi)$  of the geodesics are solved from Eq. (3) numerically. Here the initial condition is  $\phi = 0$  for  $u = 0$  in Region  $A$ , since the lights captured by the observer facing the north pole are parallel. The numerical results are illustrated in Fig. 2, where the same color denotes the same geodesic congruence in Regions  $A$  and  $A'$  respectively. It shows how the light rays enter the BH horizon in Region  $A'$  and show up from the WH horizon in Region  $A$ .

Let  $I_{\nu}^{\text{em}}$  denote the specific intensity of light from the thin disk. It is assumed to depend only on the radial  $r$ , i.e.,  $I_{\nu}^{\text{em}}(r) = I(r)$  for all  $\nu$ , where  $\nu$  is the frequency in a static frame. Consider the radiation emitted from a radius  $r_o$  in  $A'$ . Due to the symmetry of the spacetime, the history of the radiation after the turning point is the time reverse of its history before the turning point (see Fig. 1). Therefore, when it arrives at the same radius  $r_o$  in  $A$ , the light ray carries the same specific intensity and frequency as it has at  $r_o$  in  $A'$ . Since the remaining journey of the light entirely lies in  $A$ , we can employ the results in [34, 36] to conclude that the radiation will be received at some frequency  $\nu'$  with the specific intensity  $I_{\nu'}^{\text{obs}} = f(r_o)^{3/2}I(r_o)$ . Consequently, the integrand intensity  $I = \int Id\nu$  scales as  $f^2$ , i.e.,  $I^{\text{obs}} = f(r_o)^2I(r_o)$ . To understand the image of  $B'$  illuminated by the disk, we trace the null geodesics from the observer backwards towards the region near  $B'$  as in [34]. Then, the light ray may intersect with the thin disk many times and pick up the brightness repeatedly. Hence, the observed light intensity is a sum of the intensities from each intersection i.e.,  $I^{\text{obs}} = \sum_m f^2 I|_{r=r_m(b)}$ , where  $r_m(b)$  is the radial coordinate of the  $m$ th intersection of the light rays with the disk plane outside the horizon.

Whether a light ray intersects the disk is determined by the two azimuthal angles in orbital plane as the ray arrives at the horizon  $r_+$  and infinity in  $A'$ , denoted by  $\phi_{\text{out}}(b)$  and  $\phi_{\text{tot}}(b)$  respectively. Their values can be calculated numerically. According to the result shown in Fig. 3, as  $b$  increases from 0 to  $b_c$ ,  $\phi_{\text{tot}}(b)$ ,  $\phi_{\text{out}}(b)$  and the difference

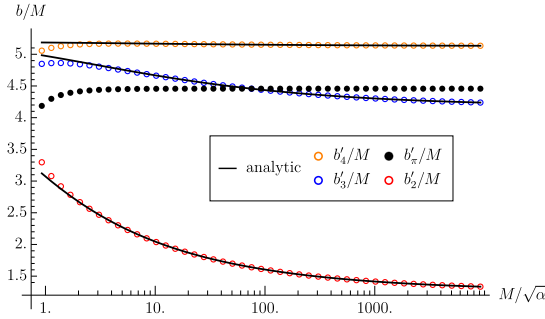


FIG. 4. The comparison of the analytic and numerical values of  $b'_n/M$  for  $n = 2, 3, 4$  and  $b_\pi/M$ .

$\Delta\phi(b) \equiv \phi_{\text{tot}}(b) - \phi_{\text{out}}(b)$  increase. To see the implication of this result to the BH image, let us start with  $b = 0$  and increase its value. As shown in Fig. 3, both  $\phi_{\text{out}}(b)$  and  $\phi_{\text{tot}}(b)$  are smaller than  $\pi/2$  at the beginning, so that these rays can not intersect with the thin disk. Then, as  $b$  increases to some value  $b_1$ ,  $\phi_{\text{tot}}(b)$  reaches  $\pi/2$  at first, so this ray and those right after could get the brightness from the thin disk. As  $b$  increases to some value  $b'_1$ ,  $\phi_{\text{out}}(b'_1)$  arrives at  $\pi/2$  while  $\phi_{\text{tot}}(b'_1)$  is smaller than  $3\pi/2$ , so that this ray and those right after cannot intersect with the disk. Hence those rays with impact factors  $b \in (b_1, b'_1)$  can intersect with the thin disk and are plotted in Fig. 2 in golden. It should be noted that in practical case the thin disk has a finite size and there is a distance between the disk and the horizon. Then not all of the light rays with  $b \in (b_1, b'_1)$  could be lightened by the disk. Those lightened rays can be finally observed in Region A as a light ring in the BH image. The analysis similar to the above can continue as the impact factor increases. As shown in Fig. 3, there exists certain value  $b_\pi$  whose corresponding light ray satisfies  $\Delta\phi(b_\pi) = \pi$ . This is the critical point such that all of the rays with  $b > b_\pi$  will intersect the equatorial plane anyway. Thus, the bright image of these rays could be continuous, in spite of that these rays may contribute bright rings in the practical cases.

The above discussions indicates that we can introduce two series of the impact factors  $b_n$  and  $b'_n$  satisfying  $\phi_{\text{tot}}(b_n) = (2n-1)\pi/2$  and  $\phi_{\text{out}}(b'_n) = (2n-1)\pi/2$  respectively to specify the edges of the bright rings. For  $M \gg \sqrt{\alpha}$ , the value of  $b_n$  and  $b'_n$  can be analytically obtained by solving Eq. (3) with  $b = \lambda M$ . To this end, we may apply the method of Matched Asymptotic Expansions [37–39], and obtain (see Appendix A for the detailed derivations)

$$\begin{aligned} \frac{\phi_{\text{tot}}(\lambda M)}{2} &= \int_0^\infty \frac{dy}{\sqrt{2y^3 - y^2 + \lambda^{-2}}} - \frac{\sqrt[6]{4\alpha\pi^3} \Gamma(\frac{5}{6})}{\Gamma(\frac{1}{3}) \sqrt[3]{M}} + O(\alpha^{1/3} M^{-2/3}), \\ \Delta\phi(\lambda M) &= \int_0^{\frac{1}{2}} \frac{dy}{\sqrt{2y^3 - y^2 + \lambda^{-2}}} + O(\sqrt{\alpha} M^{-1}), \end{aligned} \quad (4)$$

Note that the leading orders contributions to  $\phi_{\text{tot}}(\lambda M)/2$  and  $\Delta\phi(\lambda M)$  coincides with the changes of the azimuthal angles for a light traveling from  $r = \infty$  to the singularity and to the horizon in the Schwarzschild spacetime, respectively [40], since the quantum spacetime takes the Schwarzschild one as its classical limit.

The intervals  $(b_n/M, b'_n/M)$  to specify the bright rings as  $M \rightarrow \infty$  can be obtained by applying Eq. (4) and ignoring higher order terms of  $\sqrt{\alpha}/M$ . The limits of  $(b_n/M, b'_n/M)$  are  $(0.0427, 0.0445)$ ,  $(0.9242, 1.2620)$ ,  $(2.7927, 4.1766)$ ,  $(4.3175, 5.1285)$  and  $(4.9648, 5.1931)$  for  $n = 1, 2, 3, 4$  and 5 respectively. Moreover, the value of  $b_\pi/M$  as  $M \rightarrow \infty$  is solved as 4.4573. Consequently, for sufficiently large  $M$ , we have  $b'_3 < b_\pi < b'_4$ . Therefore, there are at least three discrete bright rings in the BH image for a massive BH. These rings locate at  $(b_n + b'_n)/(2M) \approx 0.04, 1.1$  and  $3.5$  respectively with widths  $\Delta b/M \approx 0.002, 0.3$  and  $1.4$ . The above results of analytical calculations are confirmed by numerical computation in their scope of application as shown in Fig. 4. It is also illustrated that  $b_\pi$  becomes smaller than  $b'_3$  for small  $M$ . Hence, there would be two distinguishable bright rings in this case.

An example of the images of the companion BH  $B'$  and the BH  $B$  is shown in Fig. 5. It illustrates that the image of  $B'$  comprises five bright rings. The first three appear distinctly in the shadow region of the image of  $B$ , while the last two are inlaid as bright rings in the illuminated region. These bright rings carry the information of QG, since they come from light rays emitting from  $B'$  and traveling through the deep Planck region  $C$ .

To summarize, the quantum extension of the Kruskal spacetime indicates that there exists a companion BH  $B'$  in a universe earlier than ours as shown in Fig. 1. We have shown that the radiation from the thin disk of  $B'$  can enter its horizon, show up from a WH horizon and contribute bright rings to the image of the BH  $B$ , as shown in Fig. 5. The overlay of the images of  $B$  and  $B'$  can be observed in our asymptotically flat region A. The positions and widths of these bright rings are also predicted precisely by our calculations. Eq. (4) implies that the leading order results

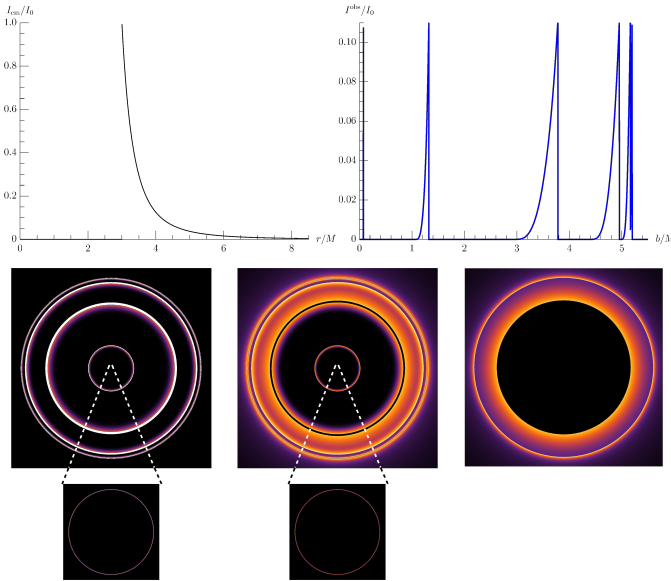


FIG. 5. The BH images: The emitting intensity of the thin disk surrounding the BH  $B'$  peaks at the photon sphere  $r_{\text{ph}} \approx 3M$  with  $M = 243.747\sqrt{\alpha}$  (the top-left panel). The observed intensity is shown in the top-right panel, and its image is given in the bottom-left panel. The image of  $B'$  comprises five distinguishable bright rings. The corresponding values of  $(b_n/M, b'_n/M)$  for  $n = 1, 2, 3, 4$  and  $5$  are  $(0.072, 0.076)$ ,  $(1.077, 1.512)$ ,  $(2.974, 4.373)$ ,  $(4.414, 5.146)$  and  $(4.995, 5.194)$ , respectively. The bottom-right panel gives the image of the BH  $B$ , also surrounded by a thin disk in the equatorial plane with the same emission as that of  $B'$ . The overlay of images of  $B$  and  $B'$  is shown in the bottom-middle panel.

are valid for a general class of quantum modified metrics with the Schwarzschild one as the classical limit, i.e., for the metric (1) with a general  $f(r)$  satisfying

$$f(wM) = 1 - \frac{2}{w} + O((\sqrt{\alpha}/M)^p), \quad (5)$$

$$f(w(\alpha M)^{1/3}) = \left( \frac{M^2}{\alpha} \right)^{1/3} F(w) + O((\sqrt{\alpha}/M)^0), \quad (6)$$

with the scaling  $r = wM$  and  $p > 0$  in (5) and with the scaling  $r = w(\alpha M)^{1/3}$  and  $F(w)$  being some function of  $w$  in (6). Equation (5) implies that the quantum modified metric returns to the Schwarzschild one in the classical regime with  $r > M$ . Equation (6) implies that the quantum corrections take the order of  $(M^2/\alpha)^{1/3}$  as  $2M/r$  in the quantum region  $r \sim (\alpha M)^{1/3}$ , where the Kretschmann scalar of the Schwarzschild spacetime approaches the Planck value. Moreover, the higher-order terms in (4) can be used to distinguish different quantum BH models satisfying the conditions (5) and (6).

The current work indicates the fantastic prediction that the BH image may encode the information of QG. It is desirable to further study this issue in more realistic models, such as the quantum Oppenheimer-Snyder model, where the emission of the matter fields falling into the BH and the absorption of the radiation by the matter fields should be both considered. It should be noted that the existence of the Cauchy horizons in the current model might lead to instability. However, it was argued that the QG effects could change the global causal structure of the spacetime and lead to a stable spacetime where BH/WH transition phenomenon would remain [41, 42]. Then our scheme would be still valid in that case. Finally, the current work opens a new window to detect the QG effects. It is interesting to note that, besides the electromagnetic radiation, the gravitational wave may also pass through the highly quantum region, bring on the information of QG, and be captured by the future observers.

## ACKNOWLEDGMENTS

C.Z. acknowledges the useful discussion with Hyat Huang, Minyong Guo, and Jinbo Yang at the early stage of this work. This work is supported by the National Natural Science Foundation of China with Grants No. 12275022, No. 11961131013, and No. 12165005.

### Appendix A: Derivation of Eq. (4)

Given an impact factor  $b = \lambda M$ , the azimuth angle  $\phi(u)$  satisfies

$$\frac{d\phi}{du} = \frac{1}{\sqrt{-\alpha M^2 u^6 + 2Mu^3 - u^2 + \beta^{-2} M^{-2}}}, \quad (\text{A1})$$

with the initial condition  $\phi(0) = 0$ . Since  $b < b_c$ ,  $G(u)$  has two roots  $u_+ > 0$  and  $u_- < 0$ . They are

$$u_+ = \left( \frac{2}{\alpha M} \right)^{1/3} - \frac{1}{6M} + O(M^{-4/3}), \quad u_- = \frac{x_0}{M} + O(M^{-2}) \quad (\text{A2})$$

where  $x_0$  is the real solution to the equation  $2\beta^2 x^3 - \beta^2 x^2 + 1 = 0$ . The domain of the (A1) is  $u \in (0, u_+)$ . Seeing  $M^{-1}$  as a perturbation, one cannot find a single asymptotic series describes  $\phi(u)$  uniformly for all values of  $u$  in the domain. We thus need to employ the Matched Asymptotic Expansion (MAE) method.

For  $u \sim u_+$ ,  $u$  is scaled by  $x = u(\alpha M/2)^{1/3}$ . Then, (A1), up to the leading order, becomes

$$\frac{d\phi_{\text{out}}}{dx} = \left( \frac{\sqrt{\alpha}}{4M} \right)^{1/3} \frac{1}{\sqrt{-x^6 + x^3}}. \quad (\text{A3})$$

The solution is

$$\phi_{\text{out}}(x) = c_1 - \left( \frac{2\sqrt{\alpha}}{M} \right)^{1/3} \frac{2F_1 \left( -\frac{1}{6}, \frac{1}{2}, \frac{5}{6}; x^3 \right)}{\sqrt{x}}, \quad (\text{A4})$$

with some integration constant  $c_1$  to be fixed.

We now come to the region  $u \sim 0$  where  $u$  is scaled by  $u = yM^{-1}$ . Then, (A1), up to the leading order, becomes

$$\frac{d\phi_{\text{in}}}{dy} = \frac{1}{\sqrt{2y^3 - y^2 + \beta^{-2}}}. \quad (\text{A5})$$

The solution to this equation is

$$\phi_{\text{in}}(u) = \frac{\sqrt[4]{3}\sqrt[6]{\Lambda}}{\sqrt[4]{\Lambda^{2/3} + \Lambda^{4/3} + 1}} \left[ F \left( \arccos \left( \frac{a_+}{a_-} \right), k \right) - F \left( \arccos \left( \frac{y - a_+}{y - a_-} \right), k \right) \right] \quad (\text{A6})$$

where the initial condition  $\phi(0) = 0$  is applied,  $F(\alpha, k)$  denotes the first kind elliptic integral

$$F(\alpha, k) = \int_0^\alpha \frac{d\theta}{\sqrt{1 - k^2 \sin^2 \theta}}, \quad (\text{A7})$$

and

$$\begin{aligned} \Lambda &= -\frac{6 \left( \sqrt{81 - 3\beta^2} - 9 \right)}{\beta^2} - 1, \quad k = \frac{1}{2} \left( \frac{\sqrt{3} (\Lambda^{2/3} + 1)}{\sqrt{\Lambda^{2/3} + \Lambda^{4/3} + 1}} + 2 \right)^{1/2}, \\ a_\pm &= \frac{-\Lambda^{2/3} - 1 + \Lambda^{1/3} \pm \sqrt{3}\sqrt{\Lambda^{4/3} + \Lambda^{2/3} + 1}}{6\sqrt[3]{\Lambda}}. \end{aligned} \quad (\text{A8})$$

By (A1), the inner solution  $\phi_{\text{in}}$  is valid for  $\alpha M^2 u^6 \ll Mu^3$ , i.e.,  $u \ll (\alpha M)^{-1/3}$ , and the outer solution is valid for  $Mu^3 \gg u^2$ , i.e.,  $u \gg M^{-1}$ . We thus have the intermedia region  $M^{-1} \ll u \ll (\alpha M)^{-1/3}$ , where the two solutions  $\phi_{\text{in}}$  and  $\phi_{\text{out}}$  match. We thus introduce  $u = cM^{-p}$  with  $1/3 < p < 1$  so that  $cM^{-p}$  lies in the intermedia region. The matching leads to

$$\lim_{M \rightarrow \infty} \phi_{\text{in}} \left( c\alpha^{1/3} M^{1/3-p} / 2^{1/3} \right) = \lim_{M \rightarrow \infty} \phi_{\text{out}}(cM^{1-p}). \quad (\text{A9})$$

which fixes  $c_1$  to be

$$c_1 = \frac{\sqrt[4]{3}\sqrt[6]{\Lambda}}{\sqrt[4]{\Lambda^{2/3} + \Lambda^{4/3} + 1}} F \left( \arccos \left( \frac{a_+}{a_-} \right), k \right) = \int_0^\infty \frac{dy}{\sqrt{2y^3 - y^2 + \lambda^{-2}}} \quad (\text{A10})$$

A uniformly valid approximation throughout the entire domain is obtained by adding the two expansion and subtracting off the common behavior. Therefore, we have

$$\begin{aligned}\phi(u) = & \frac{\sqrt{2}}{\sqrt{Mu}} - \frac{\sqrt{2} {}_2F_1\left(-\frac{1}{6}, \frac{1}{2}; \frac{5}{6}; \frac{\alpha M}{2}u^3\right)}{\sqrt{Mu}} - \frac{\sqrt[4]{3}\sqrt[6]{\Lambda}}{\sqrt[4]{\Lambda^{2/3} + \Lambda^{4/3} + 1}} F\left(\arccos\left(\frac{Mu - a_+}{Mu - a_-}, k\right)\right) \\ & + \int_0^\infty \frac{dy}{\sqrt{2y^3 - y^2 + \lambda^{-2}}}\end{aligned}\quad (\text{A11})$$

For the total change of the azimuth angle  $\phi_{\text{tot}}(\lambda M) = 2\phi(u_+)$ , a straight forward calculation gives

$$\frac{\phi_{\text{tot}}(\lambda M)}{2} = \int_0^\infty \frac{dy}{\sqrt{2y^3 - y^2 + \lambda^{-2}}} - \frac{\sqrt[3]{2}\sqrt[6]{\alpha}\sqrt{\pi}\Gamma\left(\frac{5}{6}\right)}{\Gamma\left(\frac{1}{3}\right)} \sqrt[3]{\frac{1}{M}} + O((\sqrt{\alpha}/M)^{2/3}). \quad (\text{A12})$$

For  $\phi_{\text{out}}(\lambda M) = \phi(1/r_+)$ , we have

$$\phi_{\text{out}}(\lambda M) = \int_0^{1/2} \frac{dy}{\sqrt{2y^3 - y^2 + \lambda^{-2}}} + O(\sqrt{\alpha}/M), \quad (\text{A13})$$

where  $r_+ = 2M(1 + O(M^{-1}))$  is applied.

## Appendix B: Derivation of the analytical approximation in Fig. (3)

We are concerned with the differential equation

$$\frac{d\phi}{du} = \frac{1}{\sqrt{G(u, b_c - \epsilon^2)}}, \quad (\text{B1})$$

for  $\phi(u)$ , with the initial condition  $\phi(0) = 0$  and  $\epsilon \ll \sqrt{b_c}$ . The "boundary layer" exists at  $w_c$  with  $w_c$  being the double root of  $G(w, b_c)$ . Since  $\phi_{\text{tot}}(b) = 2\phi(u_+)$  with  $u_+ > u_c$ , we need to divide the entire calculation into two part. The first part considers the solution  $\phi(u)$  for  $u \leq u_c$  to get  $\phi(u_c)$ . The second part concerns the solution  $\phi(u)$  for  $u \geq u_c$  where  $\phi(u_c)$  obtained from the previous calculation performs as the initial condition.

### 1. solution for $u < u_c$

Let us introduce  $v = u_c - u$ . Then, one gets

$$G(u_c - v, b) = \sum_{n=2}^6 \frac{1}{n!} \partial_u^n G(u_c, b_c) v^n + \frac{1}{(b_c - \epsilon)^2} - \frac{1}{b_c^2}. \quad (\text{B2})$$

For  $v = u_c - u \gg \sqrt{|\partial_u^2 G(u_c, b_c)|/b_c^3} \epsilon$ , the equation (B1) can be expand directly at  $\epsilon = 0$ . We get

$$\frac{d\phi_{\text{out}}}{du} = \frac{1}{\sqrt{G(u, b_c)}}. \quad (\text{B3})$$

Let  $v_1, v_2$  and  $v_3 \pm iv_4$  be the remaining four roots besides 0 of  $G(u_c - v, b_c)$  with

$$v_2 < 0 < u_c < v_1. \quad (\text{B4})$$

Clearly, the turning point  $u_+$  relates to  $v_2$  by  $u_+ = u_c - v_2 + O(\epsilon)$ . We introduce the real numbers  $A_1, A_2, B_1, B_2, \lambda$  and  $\beta$  with  $A_1 < 0$  such that

$$(v_1 - v)(v - v_2) = A_1(v - \lambda)^2 + B_1(v - \beta)^2, \quad (v - v_3 - iv_4)(v - v_3 + iv_4) = A_2(v - \lambda)^2 + B_2(v - \beta)^2. \quad (\text{B5})$$

Indeed, the condition  $A_1 < 0$  leads to  $B_1, A_2, B_2 > 0$ . Then, a straighforwards calculation shows that

$$\begin{aligned}\phi_{\text{out}}(u) = & \frac{k}{\sqrt{\alpha}M(\lambda - \beta)\beta\sqrt{A_2B_1}} \int_0^{\arccos\left(\sqrt{\frac{-A_1}{B_1}}\frac{u_c - u - \lambda}{u_c - u - \beta}\right)} \frac{d\theta}{\sqrt{1 - k^2 \sin^2 \theta}} \\ & - \frac{kn\lambda A_1}{\sqrt{\alpha}M\beta^3 B_1 \sqrt{A_2 B_1}} \int_0^{\arccos\left(\sqrt{\frac{-A_1}{B_1}}\frac{u_c - u - \lambda}{u_c - u - \beta}\right)} \frac{1}{1 - n \sin^2(\theta)} \frac{d\theta}{\sqrt{1 - k^2 \sin^2 \theta}} \\ & + \frac{1}{2\sqrt{\alpha}M} L\left(\frac{u_c - u - \lambda}{u_c - u - \beta}\right) + C_f^+, \end{aligned}\quad (\text{B6})$$

where  $C_f^+$  is the integration constant, the first two terms involve the elliptic integrals of the first and the third kinds respectively with

$$k = \sqrt{\frac{A_2 B_1}{A_2 B_1 - A_1 B_2}} < 1, \quad n = \frac{\beta^2 B_1}{\lambda^2 A_1 + \beta^2 B_1} > 1. \quad (\text{B7})$$

and the function  $L$  reads

$$L(t) = \frac{\ln\left(\left|\frac{\sqrt{A_2 t^2 + B_2} \sqrt{A_1 \lambda^2 + \beta^2 B_1} + \sqrt{A_1 t^2 + B_1} \sqrt{A_2 \lambda^2 + \beta^2 B_2}}{\sqrt{A_2 t^2 + B_2} \sqrt{A_1 \lambda^2 + \beta^2 B_1} - \sqrt{A_1 t^2 + B_1} \sqrt{A_2 \lambda^2 + \beta^2 B_2}}\right|\right)}{\sqrt{A_1 \lambda^2 + \beta^2 B_1} \sqrt{A_2 \lambda^2 + \beta^2 B_2}}. \quad (\text{B8})$$

In the above derivations, we applied  $B_1\beta^2 + A_1\lambda^2 = -v_1v_2 > 0$ . Moreover, it could happen that, in the second integral of  $\phi_{\text{out}}(u)$ ,  $\theta_0$  satisfying  $1 - n \sin^2 \theta$  is contained in the integration interval. In this case, the Cauchy principal value is chosen, as usually done in defining the elliptic integral. Indeed, the singularity of this integral occurs at  $u = u_c$ . Hence, if for a  $u_o < u_c$  the singularity  $\theta_0$  is contained in the integration interval  $(0, \arccos\left(\sqrt{\frac{-A_1}{B_1}}\frac{u_c - u - \lambda}{u_c - u - \beta}\right))$ , the singularity will appear to lie in  $(0, \arccos\left(\sqrt{\frac{-A_1}{B_1}}\frac{u_c - u - \lambda}{u_c - u - \beta}\right))$  for all  $u < u_c$ .

Now let us come to the inner solution  $\phi_{\text{in}}(u)$  for  $u \sim u_c$ . For  $u_c - u \ll |\partial_u^2 G(u_c, b_c)/\partial_u^3 G(u_c, b_c)|$ , we scale the variable  $v = u_c - u$  by

$$u_c - u = y\epsilon. \quad (\text{B9})$$

Then, expanding (B3) up to the leading order, one gets

$$\frac{d\phi_{\text{ini}}}{dy} = -\frac{1}{\sqrt{\alpha}M\sqrt{y^2(A_1\lambda^2 + \beta^2 B_1)(A_2\lambda^2 + \beta^2 B_2) + \frac{2}{b_c^3}}} \quad (\text{B10})$$

whose solution is

$$\phi_{\text{in}}(y) = -\frac{\text{arcsinh}\left(\sqrt{b_c^3(A_1\lambda^2 + \beta^2 B_1)(A_2\lambda^2 + \beta^2 B_2)/2}y\right)}{\sqrt{\alpha}M\sqrt{(A_1\lambda^2 + \beta^2 B_1)(A_2\lambda^2 + \beta^2 B_2)}} + C_I. \quad (\text{B11})$$

The two solutions  $\phi_{\text{in}}$  and  $\phi_{\text{out}}$  match in the intermedia region, which leads to

$$\lim_{\epsilon \rightarrow 0} \phi_{\text{ini}}(c\epsilon^{p-1}) = \lim_{\epsilon \rightarrow 0} \phi_{\text{out}}(u_c - c\epsilon^p), \quad (\text{B12})$$

with  $0 < p < 1$ . For the left hand side of (B12), we have

$$\phi_{\text{in}}(c\epsilon^{p-1}) = -\frac{\ln\left(2\sqrt{\alpha}M^2 b_c^3 (A_1\lambda^2 + \beta^2 B_1)(A_2\lambda^2 + \beta^2 B_2)/2\right) + \ln(c\epsilon^{p-1})}{\sqrt{\alpha}M\sqrt{(A_1\lambda^2 + \beta^2 B_1)(A_2\lambda^2 + \beta^2 B_2)}} + C_I. \quad (\text{B13})$$

The right hand side of (B12) is more complicated to be dealt with. We need to employ the following formula for the elliptic integrals  $\Pi(n; \phi, k)$  (see [43] Eq. 19.7.8),

$$\Pi(n; \phi, k) + \Pi(\omega; \phi, k) = F(\phi, k) + \sqrt{\xi}R_C((\xi - 1)(\xi - k^2), (\xi - n)(\xi - \omega)) \quad (\text{B14})$$

where  $\phi \in [0, \pi/2]$ ,  $n\omega = k^2$ ,  $\xi = 1/\sin^2(\phi)$  and

$$R_C(x, y) = \begin{cases} \frac{1}{\sqrt{y-x}} \arccos(\sqrt{x/y}), & 0 \leq x < y, \\ \frac{1}{\sqrt{x-y}} \ln\left(\frac{\sqrt{x} + \sqrt{x-y}}{\sqrt{y}}\right), & 0 < y < x, \\ \frac{1}{\sqrt{x-y}} \ln\left(\frac{\sqrt{x} + \sqrt{x-y}}{\sqrt{-y}}\right), & y < 0 < x. \end{cases} \quad (\text{B15})$$

By the definition of  $R_C$ , we get for  $|y| \ll 1$

$$R_C(x, y) = \frac{1}{2\sqrt{x}} (\ln(4x) - \ln(y)) + O(y). \quad (\text{B16})$$

Note that our convention defines  $\Pi(n; \phi, k) = 2\Pi(n; \pi/2, k) - \Pi(n; \pi - \phi, k)$  for  $\pi \in (\pi/2, \pi)$  so that  $\Pi(n; \phi, k)$  is  $C^1$  at  $\phi = \pi/2$ .

Taking advantage of these formulas, a straightforward calculation shows

$$\begin{aligned} \phi_{\text{out}}(u_c - c\epsilon^p) = & \frac{k}{\sqrt{\alpha}M(\lambda - \beta)\beta\sqrt{A_2B_1}} F\left(\arccos\left(\sqrt{\frac{-A_1}{B_1}}\frac{\lambda}{\beta}\right), k\right) \\ & - \frac{kn\lambda A_1}{\sqrt{\alpha}M\beta^3\sqrt{A_2B_1}} \left\{ 2\Theta(-\lambda\beta)\Pi(n, \pi/2|k) - \text{sgn}(\lambda\beta)\Pi\left(\frac{k^2}{n}, \arccos\left(\sqrt{\frac{-A_1}{B_1}}\left|\frac{\lambda}{\beta}\right|\right), k\right) \right. \\ & \left. + \text{sgn}(\lambda\beta)F\left(\arccos\left(\sqrt{\frac{-A_1}{B_1}}\left|\frac{\lambda}{\beta}\right|\right), k\right) \right\} + \frac{\ln\left(\frac{4(A_1\lambda^2 + B_1\beta^2)^2(A_2\lambda^2 + B_2\beta^2)^2}{(\beta - \lambda)^2(A_2B_1 - A_1B_2)(A_1A_2\lambda^4 + 2A_2B_1\beta^2\lambda^2 + B_1B_2\beta^4)}\right)}{2\sqrt{\alpha}M\sqrt{A_1\lambda^2 + \beta^2B_1}\sqrt{A_2\lambda^2 + \beta^2B_2}} \\ & - \frac{\ln(c\epsilon^p)}{\sqrt{\alpha}M\sqrt{(A_2\lambda^2 + \beta^2B_2)(A_1\lambda^2 + \beta^2B_1)}} + C_f^+, \end{aligned} \quad (\text{B17})$$

with  $\Theta$  denoting the step function. Thus, the matching (B12)

$$\begin{aligned} C_I = & C_f^+ + \frac{k}{\sqrt{\alpha}M(\lambda - \beta)\beta\sqrt{A_2B_1}} F\left(\arccos\left(\sqrt{\frac{-A_1}{B_1}}\frac{\lambda}{\beta}\right), k\right) \\ & - \frac{kn\lambda A_1}{\sqrt{\alpha}M\beta^3\sqrt{A_2B_1}} \left\{ 2\Theta(-\lambda\beta)\Pi(n, \pi/2, k) - \text{sgn}(\lambda\beta)\Pi\left(\frac{k^2}{n}, \arccos\left(\sqrt{\frac{-A_1}{B_1}}\left|\frac{\lambda}{\beta}\right|\right), k\right) \right. \\ & \left. + \text{sgn}(\lambda\beta)F\left(\arccos\left(\sqrt{\frac{-A_1}{B_1}}\left|\frac{\lambda}{\beta}\right|\right), k\right) \right\} + \frac{\ln\left(\frac{8\alpha Mb_c^3(A_1\lambda^2 + B_1\beta^2)^3(A_2\lambda^2 + B_2\beta^2)^3}{(\beta - \lambda)^2(A_2B_1 - A_1B_2)(A_1A_2\lambda^4 + 2A_2B_1\beta^2\lambda^2 + B_1B_2\beta^4)}\right)}{2\sqrt{\alpha}M\sqrt{A_1\lambda^2 + \beta^2B_1}\sqrt{A_2\lambda^2 + \beta^2B_2}} \\ & + \frac{\ln(\epsilon^{-2}M)}{2\sqrt{\alpha}M\sqrt{(A_1\lambda^2 + \beta^2B_1)(A_2\lambda^2 + \beta^2B_2)}}, \end{aligned} \quad (\text{B18})$$

where it should be noted that

$$\sqrt{\alpha}M\sqrt{(A_1\lambda^2 + \beta^2B_1)(A_2\lambda^2 + \beta^2B_2)} = \sqrt{\partial_u^2 G(u_c, b_c)/2}. \quad (\text{B19})$$

For  $C_f^+$ , the initial condition  $\phi_{\text{out}}(0) = 0$  leads to

$$\begin{aligned} C_f^+ = & - \frac{k}{\sqrt{\alpha}M(\lambda - \beta)\beta\sqrt{A_2B_1}} F\left(\arccos\left(\sqrt{\frac{-A_1}{B_1}}\frac{u_c - \lambda}{u_c - \beta}\right), k\right) \\ & + \frac{kn\lambda A_1}{\sqrt{\alpha}M\beta^3B_1\sqrt{A_2B_1}} \Pi\left(n; \arccos\left(\sqrt{\frac{-A_1}{B_1}}\frac{u_c - \lambda}{u_c - \beta}\right), k\right) - \frac{1}{2\sqrt{\alpha}M} L\left(\frac{u_c - \lambda}{u_c - \beta}\right). \end{aligned} \quad (\text{B20})$$

For  $u = u_c$ , one has

$$\phi(u_c) = \phi_{\text{in}}(0) = C_I. \quad (\text{B21})$$

## 2. solution for $u > u_c$

Now, let us consider  $u > u_c$ . In this region, the inner solution is

$$\phi_{\text{in}}(u) = -\frac{\operatorname{arcsinh}\left(\sqrt{\alpha M^2 b_c^3 (A_1 \lambda^2 + \beta^2 B_1) (A_2 \lambda^2 + \beta^2 B_2) / 2} (u_c - u) \epsilon^{-1}\right)}{\sqrt{\alpha M} \sqrt{(A_1 \lambda^2 + \beta^2 B_1) (A_2 \lambda^2 + \beta^2 B_2)}} + C_I. \quad (\text{B22})$$

where  $C_I$  is given by (B18). For the outer solution, we have

$$\begin{aligned} \phi_{\text{out}}(u) = & -\frac{k}{\sqrt{\alpha M}(\lambda - \beta)\beta\sqrt{A_2 B_1}} \int_0^{\operatorname{arccos}\left(\sqrt{\frac{-A_1}{B_1}} \frac{u_c - u - \lambda}{u_c - u - \beta}\right)} \frac{d\theta}{\sqrt{1 - k^2 \sin^2 \theta}} \\ & + \frac{kn\lambda A_1}{\sqrt{\alpha M} \beta^3 B_1 \sqrt{A_2 B_1}} \int_0^{\operatorname{arccos}\left(\sqrt{\frac{-A_1}{B_1}} \frac{u_c - u - \lambda}{u_c - u - \beta}\right)} \frac{1}{1 - n \sin^2(\theta)} \frac{d\theta}{\sqrt{1 - k^2 \sin^2 \theta}} \\ & - \frac{1}{2\sqrt{\alpha M}} L\left(\frac{u_c - u - \lambda}{u_c - u - \beta}\right) + C_f^-. \end{aligned} \quad (\text{B23})$$

Repeating the calculation for  $u < u_c$ , one get by matching the two solutions in the intermedia region,

$$C_f^- = 2C_I - C_f^+. \quad (\text{B24})$$

Then, the entire solution for  $u > u_c$  is

$$\begin{aligned} \phi(u) = & \frac{-k}{\sqrt{\alpha M}(\lambda - \beta)\beta\sqrt{A_2 B_1}} \int_0^{\operatorname{arccos}\left(\sqrt{\frac{-A_1}{B_1}} \frac{u_c - u - \lambda}{u_c - u - \beta}\right)} \frac{d\theta}{\sqrt{1 - k^2 \sin^2 \theta}} \\ & + \frac{kn\lambda A_1}{\sqrt{\alpha M} \beta^3 B_1 \sqrt{A_2 B_1}} \int_0^{\operatorname{arccos}\left(\sqrt{\frac{-A_1}{B_1}} \frac{u_c - u - \lambda}{u_c - u - \beta}\right)} \frac{1}{1 - n \sin^2(\theta)} \frac{d\theta}{\sqrt{1 - k^2 \sin^2 \theta}} \\ & - \frac{1}{2\sqrt{\alpha M}} L\left(\frac{u_c - u - \lambda}{u_c - u - \beta}\right) - \frac{\operatorname{arcsinh}\left(\sqrt{\alpha M^2 b_c^3 (A_1 \lambda^2 + \beta^2 B_1) (A_2 \lambda^2 + \beta^2 B_2) / 2} (u_c - u) / \epsilon\right)}{\sqrt{\alpha M} \sqrt{(A_1 \lambda^2 + \beta^2 B_1) (A_2 \lambda^2 + \beta^2 B_2)}} \\ & + \frac{\ln\left(2\sqrt{\alpha M^2 b_c^3 (A_1 \lambda^2 + \beta^2 B_1) (A_2 \lambda^2 + \beta^2 B_2) / 2}\right) + \ln((u_c - u) / \epsilon)}{\sqrt{\alpha M} \sqrt{(A_1 \lambda^2 + \beta^2 B_1) (A_2 \lambda^2 + \beta^2 B_2)}} - C_f^+ + 2C_I. \end{aligned} \quad (\text{B25})$$

The total azimuth angle is  $2\phi(u_+) = 2\phi(u_c - v_2 + O(\epsilon))$ . We thus have

$$\frac{\phi_{\text{tot}}(b_c - \epsilon^2)}{2} = -C_f^+ + 2C_I. \quad (\text{B26})$$

where we used

$$\sqrt{\frac{-A_1}{B_1}} \frac{v_2 - \lambda}{v_2 - \beta} = 1. \quad (\text{B27})$$

For  $\phi_{\text{out}}(b_c - \epsilon^2)$ , let  $v_+ = u_c - 1/r_+$  with  $r_+$  denoting the radius of the event horizon. We have

$$\begin{aligned} \phi_{\text{out}}(b_c - \epsilon^2) = & 2\phi_{\text{tot}} - \phi(u_c - v_+) \\ = & 2C_I - C_f^+ + \frac{k}{\sqrt{\alpha M}(\lambda - \beta)\beta\sqrt{A_2 B_1}} F\left(\operatorname{arccos}\left(\sqrt{\frac{-A_1}{B_1}} \frac{v_+ - \lambda}{v_+ - \beta}\right), k\right) \\ & - \frac{kn\lambda A_1}{\sqrt{\alpha M} \beta^3 B_1 \sqrt{A_2 B_1}} \Pi\left(n; \operatorname{arccos}\left(\sqrt{\frac{-A_1}{B_1}} \frac{v_+ - \lambda}{v_+ - \beta}\right), k\right) + \frac{1}{2\sqrt{\alpha M}} L\left(\frac{v_2 - \lambda}{v_2 - \beta}\right). \end{aligned} \quad (\text{B28})$$

---

[1] J. G. Polchinski, *String theory, volume I: An introduction to the bosonic string* (Cambridge university press Cambridge, 1998).

[2] A. Ashtekar, B. K. Berger, J. Isenberg, and M. MacCallum, *General relativity and gravitation: a centennial perspective* (Cambridge University Press, 2015).

[3] T. Thiemann, *Modern canonical quantum general relativity* (Cambridge University Press, 2008).

[4] T. Rothman and S. Boughn, *Foundations of Physics* **36**, 1801 (2006).

[5] F. Dyson, *International Journal of Modern Physics A* **28**, 1330041 (2013).

[6] C. Marletto and V. Vedral, *Phys. Rev. Lett.* **119**, 240402 (2017), arXiv:1707.06036 [quant-ph].

[7] J. Collins, A. Perez, D. Sudarsky, L. Urrutia, and H. Vucetich, *Phys. Rev. Lett.* **93**, 191301 (2004).

[8] A. Addazi, J. Alvarez-Muniz, R. A. Batista, G. Amelino-Camelia, V. Antonelli, M. Arzano, M. Asorey, J.-L. Atteia, S. Bahamonde, F. Bajardi, *et al.*, *Prog. Part. Nucl. Phys.* **125**, 103948 (2022), arXiv:2111.05659 [hep-ph].

[9] B. P. Abbott, R. Abbott, T. Abbott, M. Abernathy, F. Acernese, K. Ackley, C. Adams, T. Adams, P. Addesso, R. Adhikari, *et al.*, *Phys. Rev. Lett.* **116**, 061102 (2016).

[10] E. H. T. Collaboration, K. Akiyama, A. Alberdi, W. Alef, K. Asada, R. AZULY, *et al.*, *Astrophys. J. Lett.* **875**, L1 (2019).

[11] K. Akiyama, A. Alberdi, W. Alef, J. C. Algaba, R. Anantua, K. Asada, R. Azulay, U. Bach, A.-K. Baczko, D. Ball, *et al.*, *Astrophys. J. Lett.* **930**, L12 (2022).

[12] C. Liu, T. Zhu, Q. Wu, K. Jusufi, M. Jamil, M. Azreg-Aïnou, and A. Wang, *Phys. Rev. D* **101**, 084001 (2020), [Erratum: *Phys. Rev. D* **103**, 089902 (2021)], arXiv:2003.00477 [gr-qc].

[13] S. Brahma, C.-Y. Chen, and D.-h. Yeom, *Phys. Rev. Lett.* **126**, 181301 (2021).

[14] M. Afrin, S. Vagnozzi, and S. G. Ghosh, (2022), arXiv:2209.12584 [gr-qc].

[15] S. Vagnozzi *et al.*, (2022), arXiv:2205.07787 [gr-qc].

[16] J. Yang, C. Zhang, and Y. Ma, arXiv preprint arXiv:2211.04263 (2022).

[17] A. Ashtekar, J. Olmedo, and P. Singh, *Phys. Rev. Lett.* **121**, 241301 (2018), arXiv:1806.00648 [gr-qc].

[18] V. Husain, J. G. Kelly, R. Santacruz, and E. Wilson-Ewing, *Phys. Rev. Lett.* **128**, 121301 (2022).

[19] J. Lewandowski, Y. Ma, J. Yang, and C. Zhang, arXiv preprint arXiv:2210.02253 (2022), accepted for publication in *Phys. Rev. Lett.*

[20] L. Modesto, *Phys. Rev. D* **70**, 124009 (2004), arXiv:gr-qc/0407097.

[21] R. Gambini and J. Pullin, *Phys. Rev. Lett.* **101**, 161301 (2008).

[22] I. Agullo, J. Diaz-Polo, and E. Fernandez-Borja, *Phys. Rev. D* **77**, 104024 (2008), arXiv:0802.3188 [gr-qc].

[23] S. Hossenfelder, L. Modesto, and I. Prémont-Schwarz, *Phys. Rev. D* **81**, 044036 (2010).

[24] H. M. Haggard and C. Rovelli, *Phys. Rev. D* **92**, 104020 (2015).

[25] A. Corichi and P. Singh, *Class. Quant. Grav.* **33**, 055006 (2016), arXiv:1506.08015 [gr-qc].

[26] C. Zhang, Y. Ma, S. Song, and X. Zhang, *Phys. Rev. D* **102**, 041502 (2020).

[27] W.-C. Gan, N. O. Santos, F.-W. Shu, and A. Wang, *Phys. Rev. D* **102**, 124030 (2020).

[28] R. Gambini, J. Olmedo, and J. Pullin, *Classical and Quantum Gravity* **37**, 205012 (2020).

[29] K. Giesel, B.-F. Li, and P. Singh, *Phys. Rev. D* **104**, 106017 (2021).

[30] M. Han and H. Liu, *Class. Quant. Grav.* **39**, 035011 (2022), arXiv:2012.05729 [gr-qc].

[31] J. F. Barbero G., *Phys. Rev. D* **51**, 5507 (1995), arXiv:gr-qc/9410014.

[32] V. Husain, J. G. Kelly, R. Santacruz, and E. Wilson-Ewing, *Phys. Rev. D* **106**, 024014 (2022), arXiv:2203.04238 [gr-qc].

[33] J. Münch, *Phys. Rev. D* **104**, 046019 (2021), arXiv:2103.17112 [gr-qc].

[34] S. E. Gralla, D. E. Holz, and R. M. Wald, *Phys. Rev. D* **100**, 024018 (2019).

[35] J. Peng, M. Guo, and X.-H. Feng, *Phys. Rev. D* **104**, 124010 (2021), arXiv:2102.05488 [gr-qc].

[36] J. Peng, M. Guo, and X.-H. Feng, *Chin. Phys. C* **45**, 085103 (2021), arXiv:2008.00657 [gr-qc].

[37] P. A. Lagerstrom, *Matched asymptotic expansions: ideas and techniques*, Vol. 76 (Springer Science & Business Media, 2013).

[38] A. P. Porfyriadis, Y. Shi, and A. Strominger, *Phys. Rev. D* **95**, 064009 (2017).

[39] Y. Hou, P. Liu, M. Guo, H. Yan, and B. Chen, *Classical and Quantum Gravity* **39**, 194001 (2022).

[40] J. P. Luminet, *Astron. Astrophys.* **75**, 228 (1979).

[41] F. D'Ambrosio, M. Christodoulou, P. Martin-Dussaud, C. Rovelli, and F. Soltani, *Phys. Rev. D* **103**, 106014 (2021), arXiv:2009.05016 [gr-qc].

[42] M. Han, C. Rovelli, and F. Soltani, (2023), arXiv:2302.03872 [gr-qc].

[43] DLMF, “*NIST Digital Library of Mathematical Functions*,” <http://dlmf.nist.gov/>, Release 1.1.8 of 2022-12-15, f. W. J. Olver, A. B. Olde Daalhuis, D. W. Lozier, B. I. Schneider, R. F. Boisvert, C. W. Clark, B. R. Miller, B. V. Saunders, H. S. Cohl, and M. A. McClain, eds.